Transition Stage Control of Tail-Sitter Aircraft Based on Guardian Maps

ZHANG Yong[1,2*], *CHEN Xinyi*[3]

1. Research Institute of Pilotless Aircraft, Nanjing University of Aeronautics and Astronautics, Nanjing 210016, P.R. China;
2. Key Laboratory of Unmanned Aerial Vehicle Technology, Ministry of Industry and Information Technology, Nanjing University of Aeronautics and Astronautics, Nanjing 210016, P.R. China;
3. College of Computer Science and Technology, Nanjing University of Aeronautics and Astronautics, Nanjing 211106, P.R. China

(Received 18 October 2019; revised 8 March 2020; accepted 12 April 2020)

Abstract: To deal with the high nonlinearities and strong couplings in the transition stage of tail-sitter aircraft, an adaptive gain-scheduling controller is proposed by combining the guardian maps theory and H_∞ control theory. This method is applied to track the flight-path angle of the transition stage of tail-sitter aircraft, and compared with the linear quadratic regulator (LQR) method based on traditional gain scheduling. Simulation results show that the controller based on the guardian maps theory can autonomously schedule the appropriate control parameters and accomplish the stable transition. Besides, the proposed method shows better tracking performance than the LQR method based on traditional gain scheduling.

Key words: tail-sitter aircraft; transition stage; guardian maps; adaptive gain-scheduling controller

CLC number: V249.1 **Document code:** A **Article ID:** 1005-1120(2020)02-0322-10

0 Introduction

Tail-sitter aircraft is a kind of aircraft that can "sit" on the ground through tail wing[1], which makes it possible to take-off and landing vertically. During the flight, the pitch attitude of aircraft will be adjusted to 90° and the aircraft will transform into the high-speed forward flight mode. Tail-sitter aircraft combines the advantages of both rotor aircraft and fixed-wing aircraft: It can hover, maneuver around and switch to level flight in order to achieve high-speed cruise and rapid transfer in fixed-wing flight mode. Owing to the ability to switch between hovering and level flight mode, tail-sitter aircraft overcomes not only the shortcomings of fixed-wing aircraft limited by the environment but also the weaknesses of rotor aircraft with short battery life and slow speed. Compared with other vertical take-off and landing aircraft, the main advantage of tail-sitter aircraft is its simple mechanical structure. There is no need to increase the mechanism to change its power propulsion direction. In addition, it is also competitive in low failure rate, easy maintenance and so on[2-3]. Because of its advantages in task performance and structure, tail-sitter aircraft has attracted considerable attention in scientific research, civil and military fields.

The transition process of tail-sitter aircraft is a unique flight mode. In transition mode, tail-sitter aircraft will switch between horizontal cruise mode and vertical flight mode, which is also a key process for such aircraft to acquire vertical take-off and landing capability and efficient horizontal cruise capability. The difficulty lies in the strong nonlinearity and dramatic dynamic characteristic change in the whole process. It is a common way to apply gain-scheduling control strategy to deal with this kind of issue.

Osborne et al. analyzed the aerodynamic char-

*Corresponding author, E-mail address: yongzhang@nuaa.edu.cn.

How to cite this article: ZHANG Yong, CHEN Xinyi. Transition stage control of tail-sitter aircraft based on guardian maps [J]. Transactions of Nanjing University of Aeronautics and Astronautics, 2020, 37(2): 322-331.

http://dx.doi.org/10.16356/j.1005-1120.2020.02.013

acteristics of tail-sitter aircraft in detail, used gain scheduling technology in the controller design, carried out linearization analysis for the operating points of the aircraft transition flight and designed linear quadratic regulator (LQR) linear feedback control law for each operating point. Then the flight envelope was segmented and the appropriate gain scheduling strategy was designed according to the characteristics of the segmented flight envelope[4]. Batailla et al.[5]established the linear parameter varying (LPV) model to describe the transition flight process of tail-sitter aircraft and proposed a gin-scheduling controller by interpolating linear controllers for each linear time invariant (LTI) for longitudinal transition control. Besides, the preset transition trajectory is generated by using the neural network generator, and the genetic algorithm with variable environment is used to optimize the neural network instruction generator for transition trajectory optimization, so as to find the most suitable transition trajectory[6]. Knoebel et al.[7] used gain scheduling strategy of LQR controller based on the LPV model in simulation, and there are always some errors in tracking instructions in simulation experiments. Kokume et al.[8] mainly studied the controller architecture which can transform horizontal flight to hover state based on fixed-wing unmanned aerial vehicles (UAVs). The dynamic inversion controller and H_∞ controller were designed for UAV's nonlinear motion equation and the numerical simulation was carried out. Then the author studied the mathematical models of single-propeller fixed-wing aircraft in vertical take-off and vertical transition stages, designed the controllers and validated with LQR and H_∞ respectively. However, the traditional fixed-wing simulation model did not consider the effect of propeller wake on aircraft in transition and vertical states[9]. In Ref.[10], a robust formation control method was proposed to achieve the aggressive time-varying formation subject to nonlinear dynamics and uncertainties. In Ref.[11], altitude and position controllers were designed separately based on a nominal controller approach, and robust compensators were adopted to restrain the disturbances.

Since the gain scheduling method is based on each operating point of the nonlinear model, the selection of the operating point has strong subjectivity. A new operating point should be added if the dynamic characteristics of two operating points distinguish from each other. In addition, even if the controller designed at each working point performs well, control system performance during the switching process cannot be guaranteed. In another word, the global stability of the gain-scheduling controller has no theoretical proof. In order to ensure global stability and improve the conservativeness of traditional gain scheduling controller, the guardian maps theory proposed by Saydy was used[12-15]. In this paper, a linear parameter varying model of the tail-sitter aircraft is established based on the Jacobian method. The nominal H_∞ theory is adopted to design the controller at the initial point, and the guardian maps theory is used to analyze the stability boundary of the controller. Then a new controller is designed at the stability boundary, with the stability boundary calculated. The above process is repeated until the whole envelope is covered by the stability boundary. Finally, the proposed controller is used to track the flight-path angle during the tail-sitter aircraft transition process. Simulation results indicate that the controller based on the guardian maps theory can schedule the appropriate control parameters automatically and achieve satisfactory tracking performance, as well as the robustness performance, which is superior over the traditional gain scheduling method based on LQR tracking performance.

1 LPV Modeling of Tail-Sitter Aircraft

The tail-sitter aircraft studied in this paper is shown in Fig.1(a). Similar to Ref.[16], the conventional fixed-wing aircraft model is modified and the tail seat bracket is installed to achieve vertical take-off and landing. The rotors of the tail-sitter are located at the nose of the fuselage, which provides thrust for the vertical takeoff and balances the drag during the cruise. Elevons, which are located at the trailing edge of the fixed-wing, are used to control the pitch angle. The schematic diagram of the

tail-sitter flight mode is shown in Fig. 1(b). The goal of the flight control system during the vertical-to-horizontal transition is to complete the mode transformation by changing flight speed and pitch angle while keeping the yaw angle and roll angle stable[17]. According to the aircraft characteristics during the transition process, the mathematical model is decoupled, and the longitudinal kinematics model is used to design the transition controller.

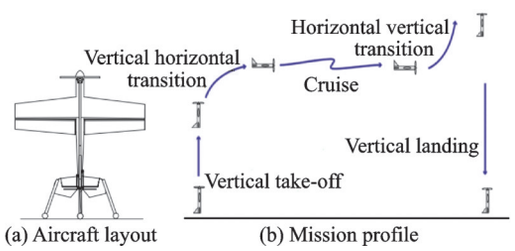

Fig.1 Flight mode of tail-sitter aircraft

As shown in Fig. 2, by decomposing the ground speed vector $\boldsymbol{V}_g$ of the aircraft, we can get the course angle between the horizontal component and the earth-surface inertial reference frame, and the flight path angle between the horizontal component and the ground speed vector $\boldsymbol{V}_g$.

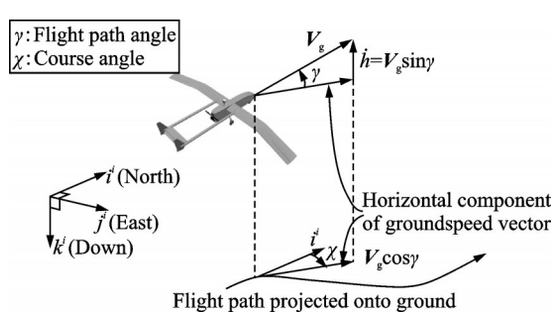

Fig.2 Flight path angle and course angle

Due to the large angle maneuver of tail-sitter aircraft during the transition process, the small-angle mathematical model will lead to singular phenomena for the large angle maneuver with pitch angle over 45°. Therefore, the horizontal Euler angle (θ) is used to describe the small-angle mathematical model, and the vertical Euler angle (θ_v) is used to parameterize the attitude matrix when the pitch angle exceeds ±45°. According to the motion mode of tail-sitter aircraft during transition flight, the mathematical model is decoupled based on level and non-sideslip flight state, and the equation of flight path angle is added to its longitudinal motion equation system to extract its longitudinal kinematics model.

During the transition between horizontal and vertical flight modes, the vertical Euler angle and the horizontal Euler angle need to be transformed. The transformation formula from horizontal Euler angle to vertical Euler angle is given as[18]

$$\begin{aligned}
\theta_v &= -\arcsin\left(\cos\phi\cos\theta\right)\\
\psi_v &= \arcsin\left(\frac{\sin\phi\cos\theta}{\cos\theta_v}\right)\\
\phi_v &= -\arcsin\left(\frac{-\sin\phi\cos\psi+\cos\phi\sin\theta\sin\psi}{\cos\theta_v}\right)
\end{aligned} \tag{1}$$

Since the horizontal Euler angle is singular when the pitch angle is 90° in vertical flight mode, the original aircraft mathematical model is transformed into a vertical Euler angle coordinate system by using the transformation formula from the horizontal Euler angle to vertical Euler angle. According to Eq. (1), the longitudinal model of the transition stage can be described by two sets of Euler angles. The longitudinal dynamic equations of the aircraft in the horizontal/vertical Euler angle inertial coordinate system are expressed as

$$\begin{cases}
\text{Horizontal}\\
\quad m\dot{V}_a = T\cos\alpha - D + mg\sin(\theta-\alpha)\\
\quad mV_a\dot{\gamma} = T\sin\alpha + L - mg\cos(\theta-\alpha)\\
\quad mV_a\dot{\alpha} = -T\sin\alpha - L + mV_a q + mg\cos(\theta-\alpha)\\
\text{Vertical}\\
\quad m\dot{V}_{a_v} = T\cos\alpha - D - mg\cos(\theta_v-\alpha)\\
\quad mV_{a_v}\dot{\gamma} = T\sin\alpha + L - mg\sin(\theta_v-\alpha)\\
\quad mV_{a_v}\dot{\alpha} = -T\sin\alpha - L + mV_a q + mg\sin(\theta_v-\alpha)\\
\quad \dot{\theta} = q\\
\quad \dot{q} = M/J_{yy}
\end{cases} \tag{2}$$

where T is the engine thrust, D the drag, L the lift, J_{yy} the moment of inertia, and M the pitching moment. In the longitudinal model of aircraft, the flight path angle γ is the main variable describing whether the aircraft is flying horizontally during the transition process. Therefore, during the controller design, the flight path angle is selected as the mission evalu-

ation criteria.

Different from nonlinear systems, LPV modeling uses linear systems with varying parameters. There are three approaches to build the LPV model: State transformation, function substitution, and Jacobian linearization. In this paper, the Jacobian linearization method is applied to establish the LPV model of tail-sitter aircraft. By linearizing the nonlinear model at the equilibrium point, a set of linearized models of the tail-sitter aircraft during the transition process can be obtained. Matrix elements are fitted into the polynomial form by means of the linear fitting method.

The range of flight speed of the tailstock aircraft studied in this paper is $V_a \in (0, 10)$ m/s. Assuming $V_a = 7$ m/s before the vertical transition, the flight state and input are decided according to the flight path angle of the aircraft. The states and control inputs at the equilibrium point are obtained by trimming the longitudinal model, then the nonlinear model is linearized to obtain the corresponding state-space model. Because of the high similarity between the linearized system and original non-linear system near the equilibrium point, the resulting LPV model is suitable for the controller design during the transition process. The data listed in Table 1 are the state variables and their inputs at the selected operating points, and $\boldsymbol{A}_n$ and $\boldsymbol{B}_n$ are the corresponding linearized state-space matrix.

Five representative operating points are selected as the input for linear parameter varying modeling. And the flight-path angle γ is taken as the scheduling parameter, and elements in the state-space matrix are fitted as the polynomial functions of the scheduling parameter. In this paper, the maximum polynomial degree is set to be 3, and the detailed polynomials are listed in Appendix A.

$$\begin{cases} \dot{\boldsymbol{X}} = \boldsymbol{A}(\gamma)\boldsymbol{X} + \boldsymbol{B}(\gamma)\boldsymbol{U} \\ \boldsymbol{Y} = \boldsymbol{C}(\gamma)\boldsymbol{X} \end{cases} \tag{3}$$

where

$$\boldsymbol{A} = \begin{bmatrix} a_{11} & 0 & a_{13} & a_{14} & 0 \\ a_{21} & 0 & a_{23} & a_{24} & 0 \\ a_{31} & 0 & a_{33} & a_{34} & 0 \\ 0 & 0 & 0 & 0 & 1 \\ 0 & 0 & a_{53} & 0 & a_{55} \end{bmatrix}, \boldsymbol{B} = \begin{bmatrix} b_{11} & 0 \\ b_{21} & b_{22} \\ b_{31} & b_{32} \\ 0 & 0 \\ 0 & b_{52} \end{bmatrix}$$

In order to verify the rationality of the established LPV model, the trajectory angle response curves of the LPV model and the non-linear model under the same step input are compared at a given trajectory angle ($\gamma = 89°$), as shown in Fig. 3.

Table 1 Trim states at different operation points

Operation point	Trim state	State-space matrix
$\gamma = 0°, V_a = 7$ m/s	$\alpha = 3.2°, \theta = 3.2°, q = 0°/s, \delta_t = 0.438, \delta_e = 0.13°$	$\boldsymbol{A}_0, \boldsymbol{B}_0$
$\gamma = 25°, V_a = 7$ m/s	$\alpha = 2.82°, \theta = 27.82°, q = 0°/s, \delta_t = 0.537, \delta_e = 0.063°$	$\boldsymbol{A}_1, \boldsymbol{B}_1$
$\gamma = 50°, V_a = 7$ m/s	$\alpha = 1.92°, \theta = 51.92°, q = 0°/s, \delta_t = 0.602, \delta_e = -0.034°$	$\boldsymbol{A}_2, \boldsymbol{B}_2$
$\gamma = 75°, V_a = 7$ m/s	$\alpha = 2.89°, \theta = 77.89°, q = 0°/s, \delta_t = 0.629, \delta_e = -0.15°$	$\boldsymbol{A}_3, \boldsymbol{B}_3$
$\gamma = 90°, V_a = 7$ m/s	$\alpha = 2.86°, \theta = 92.86°, q = 0°/s, \delta_t = 0.524, \delta_e = -0.057°$	$\boldsymbol{A}_4, \boldsymbol{B}_4$

According to the response results shown in Fig.3, the proposed LPV model of the tail-sitter aircraft matches well with the nonlinear one.

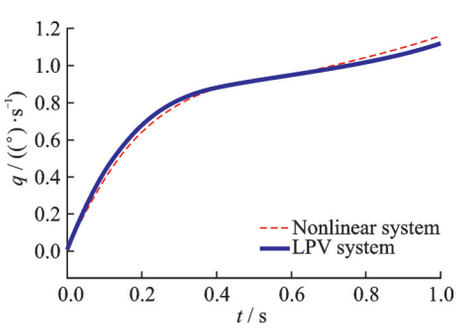

Fig.3 Step response comparison diagram

2 Adaptive Controller Design Based on Guardian Maps Theory

2.1 Guardian maps theory

Basically, guardian maps[17] are scalar-valued maps defined on the set of $n \times n$ real matrices (or nth-order polynomials) that take nonzero values on the set of "stable" matrices (or polynomials) and vanish on its boundary. The definition of guardian maps is mapping the matrix $\mathbf{R}^{n \times n}$ to a complex plane with mapping v, if $\boldsymbol{A} \in \overline{S}(\Omega)$ denotes closure of the set $\overline{S}(\Omega)$, and $\nu(\boldsymbol{A}) = 0$, then ν guards $\overline{S}(\Omega)$. The

formula is expressed as

$$\nu(\boldsymbol{A}) = 0 \Leftrightarrow \boldsymbol{A} \in S(\Omega) \tag{4}$$

The typical stability region consists of the following constraints: Region stability margin constraint, natural frequency constraint, and damping ratio constraint, as shown in Fig. 4.

If the guardian maps corresponding to respective regions are given by $v_1(\boldsymbol{A}), v_2(\boldsymbol{A}), \cdots, v_m(\boldsymbol{A})$, the guardian map for the intersection region can be written as

$$v_{\text{int}}(\boldsymbol{A}) = v_1(\boldsymbol{A}) v_2(\boldsymbol{A}) \cdots v_m(\boldsymbol{A}) \tag{5}$$

Synthesize the properties of the guardian maps and make all the eigenvalues in the open left half-plane of the complex plane. Then in the unit circle, we obtain the guardian maps which can remain the characteristic root of the system in the range of the stability margin bigger than σ and the natural frequency smaller than ω_n.

$$\begin{aligned}
&\nu_\sigma(\boldsymbol{A}) = \det(\boldsymbol{A} \odot \boldsymbol{I} - \sigma \boldsymbol{I} \odot \boldsymbol{I}) \det(\boldsymbol{A} - \sigma \boldsymbol{I}) \\
&\nu_{\omega_n}(\boldsymbol{A}) = \det(\boldsymbol{A} \odot \boldsymbol{A} - \omega_n^2 \boldsymbol{I} \odot \boldsymbol{I}) \det(\boldsymbol{A}^2 - \omega_n^2 \boldsymbol{I}) \\
&\nu_{\xi}(\boldsymbol{A}) = \det[\boldsymbol{A}^2 \odot \boldsymbol{I} + (1 - 2\xi) \boldsymbol{A} \odot \boldsymbol{A}] \det(\boldsymbol{A})
\end{aligned} \tag{6}$$

According to the synthesis property of guardian maps, the guardian map of sector region shown in Fig. 5 can be obtained as

$$\nu(\boldsymbol{A}) = \nu_\sigma(\boldsymbol{A}) \nu_{\omega_n}(\boldsymbol{A}) \nu_{\xi}(\boldsymbol{A}) \tag{7}$$

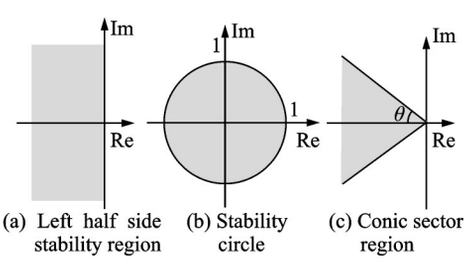

Fig.4 Basic regions

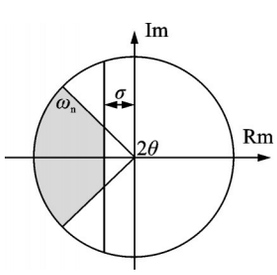

Fig.5 Classical stable region

For the unknown parameter r ranging from $r_{\min}$ to $r_{\max}$ in matrix $\boldsymbol{A}$, if $\boldsymbol{A}(r_0)$ is stable with Ω regions and ν_Ω is the guardian map of it, the maximum allowable range of parameter r in the guardian maps region can be obtained by the following procedure: Solve the value of $\nu_\Omega[\boldsymbol{A}(r)] = 0$ and the maximum real root $\underline{r}$ which has a minimum value $\nu_\Omega[\boldsymbol{A}(r)] = 0$ in the range of $[r_{\min}, r_0)$, $\underline{r} = r$ if $\nu_\Omega[\boldsymbol{A}(r)) = 0$ has no real root in $[r_{\min}, r_0)$, also solve the value of the minimum real root $\bar{r}$ which has a interval upper bound $\nu_\Omega[\boldsymbol{A}(r)] = 0$ in the range of $(r_0, r_{\max}]$, $r = r_{\max}$ if $\nu_\Omega[\boldsymbol{A}(r)] = 0$ has no real root in $(r_0, r_{\max}]$, which means the maximum stable (or unstable) interval including r_0 is $(\underline{r}, \bar{r})$.

2.2 Adaptive H_∞ controller design based on guardian maps theory

The improvement of H_∞ controller[18] design based on guardian maps theory mainly includes two aspects: One is to make the closed-loop system stable with respect to guardian maps area while satisfying the performance of H_∞; the other is to divide LPV model into several stable and controllable subsystems which can meet the performance requirements in the range of the scheduling parameters, at the same time to complete the stable operation in the whole varying process.

2.2.1 H_∞ controller design

Considering the system as shown in Fig. 6 [18]

$$\begin{cases}
\dot{\boldsymbol{X}} = \boldsymbol{A}\boldsymbol{X} + \boldsymbol{B}_1\boldsymbol{W} + \boldsymbol{B}_2\boldsymbol{U} \\
\boldsymbol{Z} = \boldsymbol{C}_{11}\boldsymbol{X} + \boldsymbol{D}_{11}\boldsymbol{W} + \boldsymbol{D}_{12}\boldsymbol{U} \\
\boldsymbol{Y} = \boldsymbol{C}_{21}\boldsymbol{X} + \boldsymbol{D}_{21}\boldsymbol{W} + \boldsymbol{D}_{22}\boldsymbol{U}
\end{cases} \tag{8}$$

where $\boldsymbol{X} \in \mathbf{R}^n$ is the state vector of the system, $\boldsymbol{W} \in \mathbf{R}^q$ the external input, $\boldsymbol{U} \in \mathbf{R}^p$ the control inputs, $\boldsymbol{Z} \in \mathbf{R}^r$ the control outputs, $\boldsymbol{Y} \in \mathbf{R}^m$ the measurable output, and $\boldsymbol{A}$, $\boldsymbol{B}_*$, $\boldsymbol{C}_*$, $\boldsymbol{D}_*$ are all real matrices with corresponding dimensions.

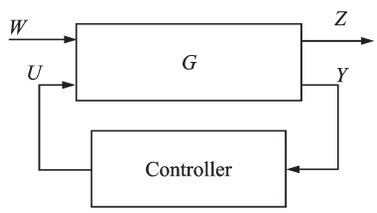

Fig.6 Block diagram of the control system

For a full-state feedback controller $\boldsymbol{U} = \boldsymbol{K}\boldsymbol{X}$, the closed-loop system is expressed as

$$\begin{cases}\dot{\boldsymbol{X}}_{\mathrm{cl}}=\boldsymbol{A}_{\mathrm{cl}}\boldsymbol{X}_{\mathrm{cl}}+\boldsymbol{B}_{\mathrm{cl}}\boldsymbol{W}\\ \boldsymbol{Z}=\boldsymbol{C}_{\mathrm{cl}}\boldsymbol{X}_{\mathrm{cl}}+\boldsymbol{D}_{\mathrm{cl}}\boldsymbol{W}\end{cases} \tag{9}$$

In order to stabilize the matrix $\boldsymbol{A}_{\mathrm{cl}}$ in Eq. (9) and ensure that there exist symmetric matrix when given the necessary and sufficient condition of performance index $\|T\|_{\infty}<\gamma$, the linear matrix inequality must satisfy

$$\begin{bmatrix}\boldsymbol{A}_{\mathrm{cl}}^{\mathrm{T}}\boldsymbol{X}_{\mathrm{cl}}+\boldsymbol{X}_{\mathrm{cl}}\boldsymbol{A}_{\mathrm{cl}} & \boldsymbol{X}_{\mathrm{cl}}\boldsymbol{B}_{\mathrm{cl}} & \boldsymbol{C}_{\mathrm{cl}}^{\mathrm{T}}\\ \boldsymbol{B}_{\mathrm{cl}}\boldsymbol{X}_{\mathrm{cl}} & -\gamma\boldsymbol{I} & \boldsymbol{D}_{\mathrm{cl}}^{\mathrm{T}}\\ \boldsymbol{C}_{\mathrm{cl}} & \boldsymbol{D}_{\mathrm{cl}} & -\gamma\boldsymbol{I}\end{bmatrix}<0 \tag{10}$$

The most used stable-mapping regions in guardian maps are represented by linear matrix inequality (LMI) regions as follows:

(1) When the guardian mapping region is a left half-plane mapping region with stability margin $|\sigma|$, where σ is the length of the imaginary axis of the stable region, and $L=2\sigma, M=1$, the necessary and sufficient condition for matrix $\boldsymbol{X}_{\mathrm{cl}}$ to make the LMI region stable is

$$\boldsymbol{A}_{\mathrm{cl}}\boldsymbol{X}_{\mathrm{cl}}+\boldsymbol{X}_{\mathrm{cl}}\boldsymbol{A}_{\mathrm{cl}}^{\mathrm{T}}+2\sigma\boldsymbol{A}_{\mathrm{cl}}<0 \tag{11}$$

(2) When the guardian mapping region is a circle region of taking the origin as the center of the circle with the radius less than ω_{n}, the necessary and sufficient condition for matrix $\boldsymbol{X}_{\mathrm{cl}}$ to make the LMI region stable is

$$\begin{bmatrix}-\omega_{\mathrm{n}}\boldsymbol{X}_{\mathrm{cl}} & \boldsymbol{A}_{\mathrm{cl}}\boldsymbol{X}_{\mathrm{cl}}\\ \boldsymbol{X}_{\mathrm{cl}}\boldsymbol{A}_{\mathrm{cl}}^{\mathrm{T}} & -\omega_{\mathrm{n}}\boldsymbol{X}_{\mathrm{cl}}\end{bmatrix}<0 \tag{12}$$

(3) When the guardian mapping region is a sector region with an angle less than 2θ, the necessary and sufficient condition for matrix $\boldsymbol{X}_{\mathrm{cl}}$ to make the LMI region stable is

$$\begin{bmatrix}\sin\theta\left(\boldsymbol{A}_{\mathrm{cl}}\boldsymbol{X}_{\mathrm{cl}}+\boldsymbol{X}_{\mathrm{cl}}\boldsymbol{A}_{\mathrm{cl}}^{\mathrm{T}}\right) & \cos\theta\left(\boldsymbol{A}_{\mathrm{cl}}\boldsymbol{X}_{\mathrm{cl}}-\boldsymbol{X}_{\mathrm{cl}}\boldsymbol{A}_{\mathrm{cl}}^{\mathrm{T}}\right)\\ \cos\theta\left(\boldsymbol{X}_{\mathrm{cl}}\boldsymbol{A}_{\mathrm{cl}}^{\mathrm{T}}-\boldsymbol{A}_{\mathrm{cl}}\boldsymbol{X}_{\mathrm{cl}}\right) & \sin\theta\left(\boldsymbol{A}_{\mathrm{cl}}\boldsymbol{X}_{\mathrm{cl}}+\boldsymbol{X}_{\mathrm{cl}}\boldsymbol{A}_{\mathrm{cl}}^{\mathrm{T}}\right)\end{bmatrix}<0 \tag{13}$$

If there exists a symmetric positive definite matrix $\boldsymbol{X}_{\mathrm{cl}}$ satisfying Eqs. (10)—(13), the closed-loop system has H_{∞} performance while maintaining the stability of the mapping region Ω.

2.2.2 Switching control design based on guardian maps

For the improvement of gain scheduling control strategy, we can refer to the guardian maps theory. Firstly, the lower boundary r_0 of the LPV model is set to the initial value of the variable parameter model, and the control law $\boldsymbol{K}_0$ satisfying Eqs. (10—13) is calculated[19].

From the equation $\nu_{\Omega}[\boldsymbol{A}_{\mathrm{aug}}(r)+\boldsymbol{B}_{\mathrm{aug}}(r)\boldsymbol{K}_0]=0$, we can calculate the scheduling parameter interval $[r_0^-, r_0^+]$ of the controller $\boldsymbol{K}_0$ that makes the system to maintain the stability in the guardian map region Ω. We regard the system model of the parameters in the interval as a subsystem. At this point, the system model of the controller $\boldsymbol{K}_0$ in the parameter range can achieve the control effect which satisfies the performance requirements. Next, r_0^+ is regarded as the initial state of the adjacent second subsystem to solve the controller $\boldsymbol{K}_1$, then this process is repeated until the scheduling parameters $r_n^+=r_{\max}$. Through this process, the LPV model can be divided into several subsystems which are stable and controllable and performance requirements satisfied in the range of scheduling parameters; each controller is regarded as the controller within the corresponding scheduling parameters, and the controller is switched on the boundary of each parameter so as to complete the stable operation of the whole changing process. The switching process of H_{∞} control law based on guardian maps is shown in Fig. 7.

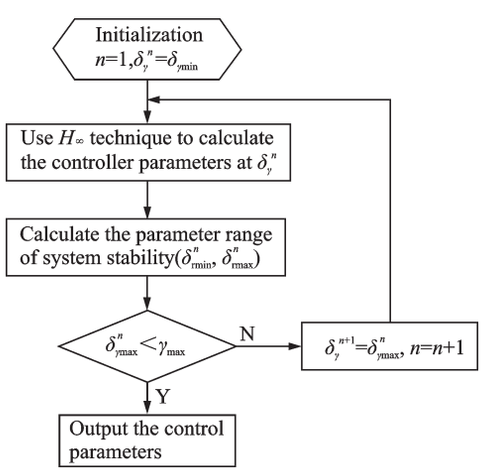

Fig.7 Flow chart of robust adaptive H_{∞} controller

3 Design and Simulation of Controller

3.1 Adaptive H_{∞} controller design of tail-sitter aircraft

In the transitional control of tail-sitter aircraft,

considering the problem of speed and flight path angle, the original system state is extended, with the speed and flight path angle errors of the aircraft added into the system state. The expected output value is $\boldsymbol{Y}_{\mathrm{r}}$ and the error between the actual output and the expected one is expressed as[20]

$$\boldsymbol{E}=\boldsymbol{Y}-\boldsymbol{Y}_{\mathrm{d}} \tag{14}$$

The integral quantity of the error is

$$\boldsymbol{X}_{\mathrm{e}}=\int_0^t\left[\boldsymbol{Y}(\tau)-\boldsymbol{Y}_{\mathrm{d}}(\tau)\right]\mathrm{d}\tau \tag{15}$$

Adding the error integration into the state equation of the LPV model yields

$$\begin{cases}\dot{\boldsymbol{X}}=\boldsymbol{A}_{\mathrm{aug}}\boldsymbol{X}_{\mathrm{aug}}+\boldsymbol{B}_{\mathrm{aug}}\boldsymbol{U}+\boldsymbol{B}_1\boldsymbol{Y}_{\mathrm{r}}\\ \boldsymbol{Y}_{\mathrm{aug}}=\boldsymbol{C}_{\mathrm{aug}}\boldsymbol{X}_{\mathrm{aug}}\end{cases} \tag{16}$$

where

$\boldsymbol{X}_{\mathrm{aug}}=[\boldsymbol{X},\boldsymbol{X}_{\mathrm{e}}]^{\mathrm{T}},\boldsymbol{A}_{\mathrm{aug}}=\begin{bmatrix}\boldsymbol{A}&0\\ \boldsymbol{C}&0\end{bmatrix},\boldsymbol{B}_{\mathrm{aug}}=[\boldsymbol{B},0]^{\mathrm{T}},\boldsymbol{B}_1=[0,-\boldsymbol{I}]^{\mathrm{T}},\boldsymbol{C}_{\mathrm{aug}}=[\boldsymbol{C},0]$.

The full-state feedback control law is designed for the augmented system, which makes $\boldsymbol{u}=\boldsymbol{K}\boldsymbol{x}_{\mathrm{aug}}$, and the closed-loop matrix of the system is expressed as $\boldsymbol{A}_{\mathrm{aug}}+\boldsymbol{B}_{\mathrm{aug}}\boldsymbol{K}$. The poles of the closed-loop system of tail-sitter aircraft are placed in a stable region. Then, the control parameters, which satisfy the stability and robustness performance index, could be calculated by solving the above LMI conditions for a positive definite symmetric matrix $\boldsymbol{X}_{\mathrm{cl}}$.

3.2 Simulation results

The proposed method is applied to design a tracking controller on flight path angle of the tail-sitter aircraft. Before the vertical to horizontal transition, the initial velocity of the aircraft is 7 m/s, and the flight path angle is 90°. After the vertical to horizontal transition, the aircraft will cruise with a constant velocity and zero flight path angle. Then, a horizontal to vertical transition will be presented. In the whole above process, the velocity is assumed to be constant.

With the predefined stability region ($|\sigma|\geqslant 2$, $\omega_{\mathrm{n}}\leqslant 6$, $\xi\geqslant 0.707$), the initial controller parameters are calculated by solving Eqs. (10)—(13) with the closed-loop system given by Eq. (17). The resulting initial controller $\boldsymbol{K}_0$ is given by

$$\boldsymbol{K}_0=\begin{bmatrix}-0.376&0.015\\ -0.03&-0.206\\ 0.136&-0.045\\ 0.201&-0.003\\ -4.376&-0.006\\ -4.746&0.003\\ -0.031&-0.589\end{bmatrix}^{\mathrm{T}} \tag{17}$$

Then, the stability boundary of the initial controller is calculated by setting $\nu_{\Omega}[\boldsymbol{A}_{\mathrm{aug}}(r)+\boldsymbol{B}_{\mathrm{aug}}(r)\boldsymbol{K}_0]$, resulting in $r\in(0,1.13)$. The stable scheduling parameters of the system are used to calculate the controller again until the boundary of the parameter covers the whole control process. Finally, two sets of controllers are obtained, and the parameter scheduling range that makes the system about the guardian mapping region Ω stable is $(-1.336\,1,0.53)$, $(0.280\,4,2.214)$.

$$\boldsymbol{K}_1=\begin{bmatrix}-0.517&0.000\,3\\ -0.002&-0.368\\ 0.134&-0.148\,8\\ 0.201&-0.006\\ 0.000\,3&-0.007\,9\\ 0&0.008\,2\\ -0.041\,3&-1.309\,2\end{bmatrix}^{\mathrm{T}} \tag{18}$$

The controller parameters switch at the midpoint of the intersectional stability regions. We apply the control parameters into five equilibrium points to observe the pole distribution. The pole distribution of the aircraft in open and closed-loop cases is shown in Fig.8. According to Fig.8, the adaptive H_∞ controller based on guardian maps can obtain predictable flight quality.

To compare the proposed adaptive H_∞ controller based on guardian maps with the traditional gain scheduling LQR controller, the LQR control law is designed at five equilibrium points for the established LPV model, and the gain scheduling control technology is applied to the nonlinear simulation.

We put forward an adaptive H_∞ controller based on guardian maps and the simulation results are compared with the traditional gain scheduling

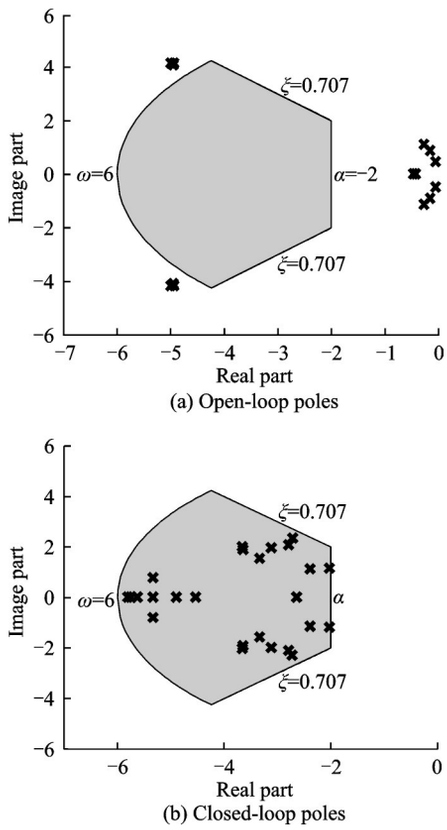

Fig.8 Pole distribution comparison diagram

LQR controller. The linear speed V_a is set to 7 m/s, the initial flight path angle is 90°, the pitch is 90°, the input command is flight path tracking, the slope is −1 (°/s), the ramp signal is limited by 90°, the input speed command is 7, and the simulation time is 100 s. The simulation results are shown in Fig. 9.

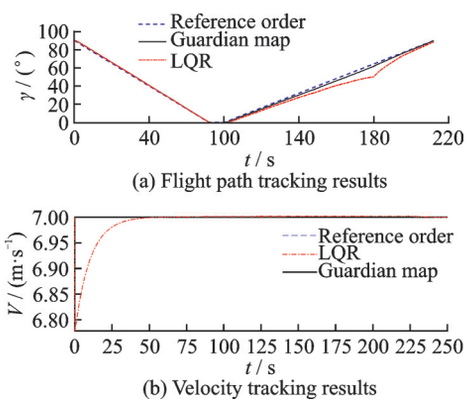

Fig.9 Command tracking comparison diagram

According to the simulation results of Fig. 9, when LQR is used to track the flight path angle, there is a certain lag and overshoot in flight path angle tracking and a certain fluctuation of aircraft attitude at the beginning and end of the transition, and airspeed tracking also has some errors. Meanwhile, there is no lag and overshoot in flight path angle tracking when we use adaptive H_∞ controller based on guardian maps, and airspeed tracking has no errors either. Moreover, the control by LQR cannot guarantee the flight speed to be maintained in the axial direction, which will produce large components in the other two axes. But this phenomenon will not occur in the guardian maps control. In addition, the computer running time is 30 min when LQR is used for tracking simulation, while the H_∞ gain scheduling controller designed by guardian maps theory runs for 2 min when tracking simulation is carried out.

Furthermore, the robustness of the proposed controller is verified. Assuming the uncertainties associated with aerodynamic coefficients are within 20% on account of external disturbance, the flight path angle and velocity tracking results of Monte Carlo simulation are shown in Figs.10, 11.

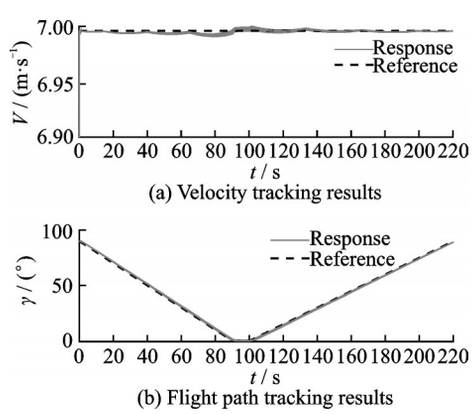

Fig.10 Command tracking with 20% uncertainty

According to Fig.11, the throttle angle and elevator deflection at the input end of H_∞ gain scheduling controller based on the guardian maps theory is within the acceptable range. And the H_∞ gain scheduling controller based on the guardian maps theory can effectively control the transition of the tailstock air-sitter and guarantee the satisfactory flight quality.

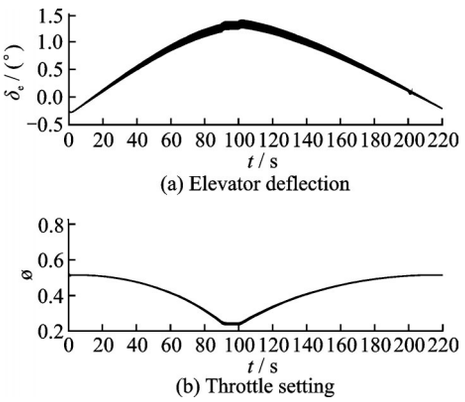

Fig.11 Control input under 20% uncertainty

4 Conclusions

A guardian map based adaptive robust H_∞ controller is proposed for the tail-sitter control during the transition phase, which simultaneously satisfies the stability and robust performance requirements. Then, the proposed method is applied to the longitudinal nonlinear model of tail-sitter aircraft to track the flight path angle at fixed airspeed. Compared with the traditional LQR based gain scheduling method, simulation results indicate that the gain scheduling controller designed by the proposed method achieves satisfactory tracking performance in the transition region. In addition, different from LQR, the proposed method guarantees the global stability of the resulting scheduling controller.

Appendix A

$a_{11}=-0.67\gamma^3+0.81\gamma^2-0.14\gamma-1.13$

$a_{13}=54.47\gamma^3-70.14\gamma^2+11.84\gamma-5.55$

$a_{14}=-59.95\gamma^3-74.19\gamma^2-13.58\gamma-9.68$

$a_{21}=0.49\gamma^3-0.60\gamma^2+0.10\gamma+0.08$

$a_{23}=11.7$

$a_{24}=-2.39\gamma^3+1.90\gamma^2+0.73\gamma+0.32$

$a_{31}=-0.49\gamma^3+0.60\gamma^2-0.10\gamma-0.08$

$a_{33}=-11.7$

$a_{34}=2.39\gamma^3-1.90\gamma^2-0.73\gamma-0.32$

$a_{53}=-69.9$

$a_{55}=-8.38$

$b_{11}=-49.56\gamma^3+30.18\gamma^2+26.86\gamma-38.08$

$b_{21}=1.07\gamma^3-1.43\gamma^2+0.36\gamma+0.15$

$b_{22}=-1.21$

$b_{31}=-1.07\gamma^3+1.43\gamma^2-0.36\gamma-0.15$

$b_{32}=1.21$

$b_{52}=625.56$

References

[1] LI Z Y, ZHANG L X, LIU H, et al. Nonlinear robust control of tail-sitter aircrafts in flight mode transitions[J]. Aerospace Science & Technology, 2018, 81: 348-361.

[2] SALAZAR G, CASTILLO P, WONG K C, et al. Attitude stabilization with real-time experiments of a tail-sitter aircraft in horizontal fight[J]. Journal of Intelligent and Robotic Systems, 2012, 65(1/2/3/4): 123-136.

[3] LIU H, PENG F C, FRANK L, et al. Robust tracking control for tail-sitters in flight mode transitions[J]. IEEE Transactions on Aerospace & Electronic Systems, 2019, 55(4): 2023-2035.

[4] KNOEBEL N, OSBORNE S, SNYDER D, et al. Preliminary modeling , control, and trajectory design for miniature autonomous tailsitters[C]//Proceedings of AIAA Guidance, Navigation, and Control Conference and Exhibit. Colorado: AIAA, 2006: 1-12.

[5] BATAILLA B, MOSCHETTA J M, POINSOT D, et al. Development of a VTOL mini UAV for multi-tasking missions[J]. Aeronautical Journal, 2009, 113(1140): 87-98.

[6] KUBO D, SUZUKI S. Robust optimal autopilot design for a tail-sitter unmanned aerial vehicle[J]. Journal of Aerospace Computing, Information, and Communication, 2008, 5(5): 135-154.

[7] KNOEBEL N B, MCLAIN T W. Adaptive quaternion control of a miniature tailsitter UAV[C]//Proceedings of IEEE American Control Conference. Washington: IEEE, 2008: 2340-2345.

[8] KOKUME M, UCHIYAMA K. Control architecture for transition from level flight to hover of a fixed-wing UAV[C]//Proceedings of Conference on IEEE Industrial Electronics Society. Melbourne: IEEE, 2011: 522-527.

[9] CASAU P, CABECINHAS D, SILVESTRE C. Almost global stabilization of a vertical take-off and landing aircraft in hovered flight[C]//Proceedings of American Control Conference. Montreal: IEEE, 2012: 3247-3252.

[10] LIU D, LIU H, LEWIS F L, et al. Robust time-varying formation control for tail-sitters in flight mode transitions[J]. IEEE Transactions on Systems, Man, and Cybernetics: Systems, 2019. DOI: http://doi. org/

10.1109/TSMC.2019.2931482.

[11] LI Z, ZHOU W, LIU H, et al. Nonlinear robust flight mode transition control for tail-sitter aircraft[J]. IEEE Access, 2018, 6: 65909-65921.

[12] XIAO D B, LIU M Y, LIU Y B, et al. Switching control of a hypersonic vehicle based on guardian maps [J]. Acta Astronautica, 2016, 122: 294-306.

[13] SAUSSIE D, SAYDY L, AKHRIF O, et al. Gain scheduling with guardian maps for longitudinal flight control[J]. Journal of Guidance, Control and Dynamics, 2011, 34(4): 1045-1059.

[14] LI C L, LIU Y B, PENG F J, et al. An adaptive parameter regulation algorithm for control systems based on guardian maps theory[J]. Information and Control, 2014, 43(2): 193-198, 204. (in Chinese)

[15] LIU Y B, LIU M Y, SUN P H. Robust stabilization control based on guardian maps theory for a longitudinal model of hypersonic vehicle[J]. The Scientific World Journal, 2014. DOI: https:// doi. org/10.1155/2014/270172.

[16] MATSUMOTO T, KITA K, SUZUKI R, et al. A hovering control strategy for a tail-sitter VTOL UAV that increases stability against large disturbance[C]// Proceedings of IEEE International Conference on Robotics & Automation. Anchorage: IEEE, 2010: 54-59.

[17] FORSHAW J L, LAPPAS V J, BRIGGS P. Transitional control architecture and methodology for a twin rotor tailsitter[J]. Journal of Guidance, Control, and Dynamics, 2014, 37(4): 1289-1298.

[18] MOHAMMED T O, ELKHMRI N M, ELKHMRI H. Analysis and simulation of UAV aircraft flight dynamics [J]. Advanced Materials Research, 2014, 915: 7-11.

[19] DONG W H, YAN Y Y, XIE W J, et al. Performance-oriented state-feedback controller parameter tuning with guardian maps[J]. International Journal of Control Automation and Systems, 2016, 14 (3): 773-778.

[20] LIA X J, YANGAB G H. Adaptive H_∞ control in finite frequency domain for uncertain linear systems[J]. Information Sciences, 2015, 314: 14-27.

Acknowledgement This work was supported by the Fundamental Research Funds for the Central Universities (No. NJ2018015).

Author Mr. **ZHANG Yong** received his M. S. degree in Navigation, Guidance and Control from Nanjing University of Aeronautics and Astronautics (NUAA) in 2012. His research is related to integrated design of artificial intelligence and flight control of UAVs.

Author contributions Mr. **ZHANG Yong** contributed to designing the study and programming the new algorithm, conducted the analysis, interpreted the result, and wrote the manuscript. Ms. **CHEN Xinyi** contributed to the discussion and background of the study. All authors commented on the manuscript draft and approved the submission.

Competing interests The authors declare no competing interests.

(Production Editor: WANG Jing)

基于保护映射的尾坐式飞行器过渡过程控制

张 勇[1,2], 陈辛怡[3]

(1.南京航空航天大学无人机研究院,南京 210016,中国; 2.南京航空航天大学中小型无人机先进技术工业和信息化部重点实验室,南京 210016,中国; 3.南京航空航天大学计算机科学与技术学院,南京 211106,中国)

摘要:针对尾座式飞行器过渡阶段动力学模型的大范围非线性变化问题,结合保护映射理论和H_∞控制理论设计自适应控制增益调度技术。将提出的自适应控制增益调度技术对尾座式飞行器过渡过程的纵向模型进行航迹角跟踪,并与传统的基于增益调度技术的LQR方法进行对比。仿真结果表明:基于保护映射理论设计的控制器能够自主切换合适的控制律,完成过渡过程的稳定转换,并且本文方法比基于传统增益调度技术的LQR方法显示出了更好的跟踪性能。

关键词:尾座式飞行器;过渡过程;保护映射;自适应增益调度控制器